

# Sparse Mixers: Combining MoE and Mixing to build a more efficient BERT

James Lee-Thorp and Joshua Ainslie

Google Research

{jamesleethorp, jainslie}@google.com

## Abstract

We combine the capacity of sparsely gated Mixture-of-Experts (MoE) with the speed and stability of linear, mixing transformations to design the Sparse Mixer encoder model. The Sparse Mixer slightly *outperforms* ( $<1\%$ ) BERT on GLUE and SuperGLUE, but more importantly trains 65% faster and runs inference 61% faster. We also present a faster variant, prosaically named Fast Sparse Mixer, that marginally *underperforms* ( $<0.2\%$ ) BERT on SuperGLUE, but trains and runs nearly twice as fast: 89% faster training and 98% faster inference. We justify the design of these two models by carefully ablating through various mixing mechanisms, MoE configurations and model hyperparameters. The Sparse Mixer overcomes many of the latency and stability concerns of MoE models and offers the prospect of serving sparse student models, without resorting to distilling them to dense variants.<sup>1</sup>

## 1 Introduction

Sparsely gated Mixture-of-Experts (MoE) models have seen a surge of interest in recent years (Shazeer et al., 2017; Lepikhin et al., 2021; Fedus et al., 2022; Riquelme et al., 2021; Artetxe et al., 2021; Clark et al., 2022). These MoE models offer the promise of sublinear compute costs with respect to the number of model parameters – by training "experts" that can independently process different slices of input data, MoE sublayers can increase the capacity of models with only limited increases in FLOPS.

Perhaps because of the favorable capacity-to-compute trade-off, many recent MoE studies, including most of the aforementioned studies, have focused on using MoE to scale up large models. The task of serving these models in practice is either largely ignored or relegated to a knowledge

distillation setup wherein a sparse teacher model is distilled to a dense student model, often with a significant quality loss relative to the sparse teacher model. For example, Fedus et al. (2022) are only able to distill 30% of the Switch Transformer's quality gains to a dense model.

Another recent direction of work is mixing models (Tolstikhin et al., 2021; Lee-Thorp et al., 2021). These models replace attention in Transformer-like models with simpler linear transformations or MLP blocks that "mix" input representations. Linear transformations are particularly attractive because they are faster than the combined projection and dot product operations in an attention sublayer.

In this work, we pull on both MoE and mixing threads to build low latency, sparse encoder models that can be used in production settings. We opt to focus on encoder models, and BERT-like models in particular, because they are widely used in practice – for example, in dual encoder setups for retrieval (Bromley et al., 1993; Karpukhin et al., 2020).

Relative to the vanilla, dense Transformer model (Vaswani et al., 2017), we speed up our model in two ways: (1) We use the increased capacity from MoE sublayers to offset parameter reductions in other parts of the model. (2) We use mixing transformations to replace a large fraction of self-attention sublayers with faster linear transformations. The resulting model, which we name Sparse Mixer, slightly ( $< 1\%$ ) *outperforms* BERT on GLUE (Wang et al., 2018) and SuperGLUE (Wang et al., 2019), but most importantly trains 65% faster and runs inference 61% faster. We also introduce a simple variant of Sparse Mixer, prosaically named Fast Sparse Mixer, that marginally ( $< 0.2\%$ ) *underperforms* BERT on SuperGLUE, but runs nearly twice as fast: training 89% faster and running inference 98% faster.

One interesting finding of our work is a training stability synergy between the sparse and mixing model components. Sparse models are typically

<sup>1</sup>Code will soon be made available at [https://bit.ly/sparse\\_mixers](https://bit.ly/sparse_mixers).

prone to instability during training (Zoph et al., 2022). For example, we find that simply replacing dense feed-forward sublayers in BERT with MoE variants yields highly unstable models; see Section 4.3. However, these instabilities dissipate as we replaced self-attention sublayers with mixing sublayers. We hypothesize that the (token-dependent) relevance weighted self-attention operation is the source of the instability, and hence that replacing the majority of self-attention sublayers with mixing sublayers, renders sparse mixer models highly stable.

In summary, the contributions of our paper are as follows.

- We introduce Sparse Mixer, a model that matches BERT on GLUE and SuperGLUE but runs 61-65% faster.
- We introduce a faster variant of Sparse Mixer ("Fast Sparse Mixer") that very slightly underperforms BERT ( $< 0.2\%$ ) but that runs nearly twice as fast.
- We demonstrate that speed and stability regressions of MoE models may be overcome using mixing mechanisms. Importantly, this shows that we may directly serve sparse models, rather than resorting to distilling them to dense variants.
- We ablate a large number of settings covering the model mixing configuration, the model MoE configuration, and the overall model shape to justify the design of the Sparse Mixer.

## 2 Related work

### 2.1 Sparsely gated Mixture-of-Experts

Mixture-of-Experts (MoE) models were introduced by Jacobs et al. (1991); Jordan and Jacobs (1994) and more recently popularized by Shazeer et al. (2017). Recent work, such as (Zoph et al., 2022), has played out the promise of MoE models by achieving SOTA results on a number of NLP benchmarks. As with the majority of recent MoE works, these models are large with a focus on model quality. When efficiency is studied, it is typically at the level of a total train time efficiency metric. For example, although the per training step speed of the Switch Transformer (Fedus et al., 2022) is slower than the vanilla, dense Transformer, because the Switch Transformer accuracy curves reach a higher

accuracy faster than the dense model, the Switch Transformer can be correctly described as a more efficient model. However, the slower step speed is an Achilles heel for serving such models; for low latency settings, one generally cannot ask a user to wait longer for a more accurate model response.

A notable exception to total training time efficiency studies is Jaszczur et al. (2021), who sparsify multiple components of the Transformer to achieve an order of magnitude increase in inference speed. However, they are only able to demonstrate these gains for the particular setting of unbatched inference on CPUs, and the speed-ups do not carry over to training. MoE algorithms, in contrast, offer a more hardware accelerator friendly sparse algorithm as each expert performs dense matrix multiplications. In this work, we focus on both training and inference step speed metrics. Moreover, we seek a model that is more efficient not because its final accuracy asymptotes at a higher value than dense model counterparts, but because the model architecture actually processes input examples quickly.

Another important aspect to training MoE models is that they are often prone to instability during training. Several techniques have been introduced to remedy this such as decreasing the learning rate or applying gradient clipping, however, many of these modifications often lead to quality regressions (Zoph et al., 2022). In our encoder setup, we are able to stabilize our MoE encoder models by replacing the majority of self-attention sublayers with mixing sublayers that perform simple linear transformations of the input.

Memory mechanisms are another popular sparse technique for adding capacity to models with limited increases in compute costs; see, for example, (Weston et al., 2015; Sukhbaatar et al., 2015; Lampl et al., 2019). While both intuitively appealing and empirically promising, memory techniques have a few drawbacks that make them less attractive to our study: (1) modular setups, wherein the memory block must either be maintained separately or carefully tuned alongside dense model components, and (2) suboptimal implementations (lookups in particular) for accelerator hardware often yield models that have favorable theoretical compute properties, but are slow in practice.

### 2.2 Mixing

Several recent works have explored mixing mechanisms, such as single matrix multiplications (Tay

et al., 2020; Lee-Thorp et al., 2021), MLP blocks (Tolstikhin et al., 2021) and spectral transforms (Lee-Thorp et al., 2021), as an efficient replacement of attention sublayers in Transformer-like models. Of particular relevance to our work, Lee-Thorp et al. (2021) found that hybrid attention-mixing models, wherein only a small number of attention sublayers were retained, yielded models that were faster than BERT with only a limited degradation to accuracy. We build off this observation and use sparse MLP sublayers to compensate for the remaining accuracy gap.

Mixing models overlap with a large class of works designing approximate attention mechanisms that scale more favorably with longer input sequences than vanilla attention; see (Tay et al., 2021a) for a survey of these methods. We suspect that the Sparse Mixer model could be adapted to long sequence settings by (a) replacing the few attention sublayers with efficient ones and (b) selecting for mixing mechanisms that scale most favorably with longer sequences, such as spectral transforms implemented using Fast Fourier Transforms (FFTs) (Lee-Thorp et al., 2021).

### 2.3 Model shape

Scaling up models has proven to be a successful program for increasing model quality (Kaplan et al., 2020; Raffel et al., 2020; Brown et al., 2020). The relationship between the number of model parameters and model quality can be roughly modelled through a power law (Kaplan et al., 2020; Clark et al., 2022). However, the configuration of these parameters within the model also plays an important role in model quality and efficiency. Consistent with Tay et al. (2021b), we find that making the model thinner (smaller model and activation dimensions) but potentially longer (more layers) is generally an efficient way to distribute parameters throughout the model.

## 3 Model

### 3.1 Architecture

Our design space for the Sparse Mixer builds off the Transformer encoder architecture (Vaswani et al., 2017), with layers of stacked encoder blocks; see Figure 1. Each encoder block contains a mixing sublayer and an MLP sublayer, connected with residual connections and layer norms. We keep the standard BERT input embedding and output projection layers (Devlin et al., 2019).

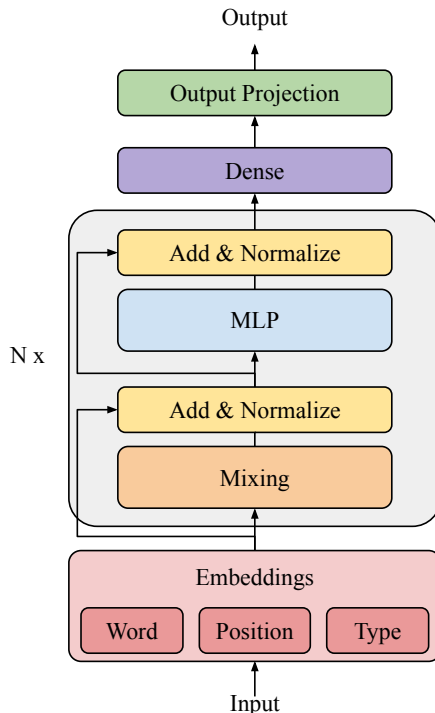


Figure 1: Block based encoder architecture. The model has  $N$  encoder blocks, each containing mixing and MLP sublayers. Each MLP sublayer may be sparse or dense. Each mixing sublayer may use self-attention or a mixing transformation.

We arrive at our final architecture by carefully ablating through mixing mechanisms, MoE configurations and model shape hyperparameters in Section 4.1. The resulting optimized encoder blocks are shown in Figure 2.

### 3.2 MoE

When training a dense model layer over multiple devices, the first tool we reach for is data parallelism: we replicate our layer over all devices and perform the same model computations in parallel over separate shards of the data. In contrast, when training an MoE layer over multiple devices, we use data and expert parallelism: we initialize multiple, different instances ("experts") of our layer over the devices and perform parallel computations with each instance over separate shards of the data.

Importantly, there is a trade-off between these two setups: the MoE layer has more capacity than the dense layer but each parameter receives less training signal. Indeed, the number of model parameters scales proportionally with the number of experts, but the gradient update for an individual sparse parameter is accumulated over less data rela-

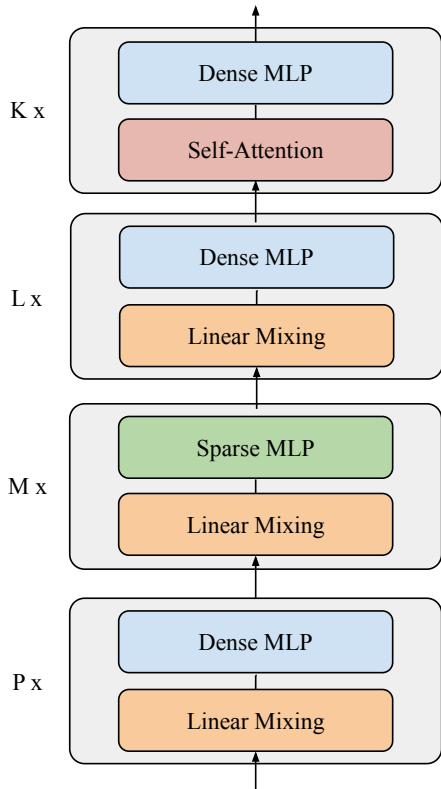


Figure 2: Sparse Mixer architecture for the Base configuration. For display clarity, layer norms, residual connections, embedding layers and output layers are not shown. The top  $K = 4$  blocks contain self-attention and dense MLP sublayers; the middle  $M = 4$  blocks contain mixing and sparse MLP sublayers; and the remaining  $L = 1$  and  $P = 5$  blocks contain mixing and dense MLP sublayers.

tive to the replicated parameters of the dense layer.<sup>2</sup>

Generalizing from a particular layer to the entire model, we may interleave dense/replicated components (e.g. attention or layer norms) with the sparse MoE components (MLP blocks in this work). The number of experts in a given sparse MoE layer may be greater than the number of devices. As we increase the number of experts, we typically decrease the *expert capacity* – the number of tokens processed by an individual expert. More specifically, with  $E$  denoting the number of experts and  $n$  the number of tokens, we set

$$\text{expert capacity} = cf \times n/E,$$

where  $cf$  is the scalar *capacity factor*. For  $cf \approx 1$ , this allows us to increase model parameter count with minimal increases in FLOPS.<sup>3</sup>

<sup>2</sup>In this work, we ignore model parallelism, an important technique for partitioning large models over multiples devices.

<sup>3</sup>Modulo increased FLOPS from the token assignment

### 3.2.1 Routing

Rather than randomly sharding data between experts, we use a *router*, also known as a gating function, to carefully direct data shards between experts. This follows the intuition that expert A may become specialized at processing inputs in one part of the embedding space, while experts B, C, ... are specialized to other parts of the embedding space.

Router design is an active research area; see, for example, (Lewis et al., 2021; Roller et al., 2021; Zhou et al., 2022; Clark et al., 2022). We limit ourselves to two router types: traditional top-k "Tokens Choose" and "Experts Choose". We follow the standard practice of routing at the token level – the router assigns each token to a subset of experts. Both assignment algorithms start from the same place: token representations are mapped by a router weight matrix from the embedding dimension,  $d_m$ , to the expert dimension,  $E$ :

$$\mathcal{W} : \mathbb{R}^{d_m} \mapsto \mathbb{R}^E.$$

The resulting router logits are normalized to a probability along the last ( $E$ ) axis using a softmax. Tokens are then assigned to experts differently, depending on the assignment algorithm.

If the router logits blow up, the MoE model will become unstable. To encourage the model to produce small router logits, Zoph et al. (2022) introduce a router z-loss. We include the router z-loss in our study, with the recommended  $10^{-3}$  scaling factor, although we do not observe instability issues without the router z-loss.

### 3.2.2 Tokens Choose routing

In top-k Tokens Choose routing (Shazeer et al., 2017), each token is assigned to its top-k experts. As we are primarily interested in efficiency, we use top-1 ("Switch") routing (Fedus et al., 2022).

Working our way through each token in the batch, we may eventually find that a given token will fail to be routed to its chosen experts if those experts' capacities have been reached. There is no guarantee that each token is processed by an expert, although any token that fails to reach an expert will still propagate into the next encoder block through the residual connection. There is also no guarantee that each expert receives at least one token for that matter. To combat this and ensure that compute is efficiently distributed among experts, we include

algorithm; see Section 3.2.1. For few experts, the associated FLOPS increase from routing assignment is relatively small.



the load balancing loss as in (Shazeer et al., 2017; Fedus et al., 2022; Zoph et al., 2022).

We can increase expert capacity by increasing the capacity factor,  $cf$ . This will increase the probability that a given token is routed to its desired experts. Decreasing the capacity factor will further sparsify the model and speed up the MoE sublayer.<sup>4</sup> Following Riquelme et al. (2021), we also use Batch Prioritized Routing (BPR) for Tokens Choose routing. With BPR, we prioritize routing those top-k tokens with the highest router probability, rather than simply routing tokens on the typical left-to-right ordering in which they appear in the batch.

### 3.2.3 Experts choose routing

The Experts Choose assignment algorithm was introduced by Zhou et al. (2022). Here, experts choose their top tokens, rather than tokens choosing experts; this effectively amounts to a transpose of the router probabilities prior to the top-k operation. Each expert performs its top-k operation with  $k = \text{expert capacity}$ . An individual token may be processed by multiple experts or none at all. Because experts have their choice of tokens and always fill their buffer, increasing the capacity factor,  $cf$ , will increase both the number of tokens that an expert processes AND indirectly the number of experts that a given token is routed to. Because experts choose their tokens and each expert always fills its capacity, no auxiliary loading balance loss is required for Experts Choose routing.

### 3.2.4 Token group size

Tokens are subdivided into groups and expert assignment is performed on a per-group basis. A larger group size will result in slower but more accurate top-k and sorting computations, whereas a smaller group size will result in faster but more approximate (and potentially less stable) routing choices. In practice, we find that imperfect routing choices are tolerable and start our study with a group size of 4096 tokens.

## 3.3 Mixing

We use simple linear, mixing transformations as drop-in replacements of self-attention sublayers.

<sup>4</sup>We can also introduce separate train and evaluation capacity factors. A natural technique often employed in MoE models is to set  $cf_{\text{eval}} > cf_{\text{train}}$  to improve inference quality without slowing down training; see, for example, (Zoph et al., 2022). In our study, we fix  $cf_{\text{eval}} = cf_{\text{train}}$  as we prioritize inference speed.

Mixing transformations offer speed for reduced capacity and flexibility. Indeed, the attention mechanism contains four parameterized projections and two dot product operations ("QK" and "V"), allowing self-attention sublayers to construct representations in a highly expressive, token-dependent basis. On the other hand, all of the mixing transformations we investigate are implemented through two projections, one along each of the sequence and model dimensions. Moreover, the mixing weights are token-independent. Fixing the mixing basis, relative to different data inputs, turns out to be helpful as it stabilizes the model during training. That said, in Section 4.1.1, we find that the most Pareto efficient models are hybrid models that include both mixing and some self-attention sublayers.

### 3.3.1 Spectral transformations

We experiment with the Fourier and Hartley transforms, which showed the most promise of the spectral transforms studied by Lee-Thorp et al. (2021). We integrate these transforms through a Fourier or Hartley sublayer. The Fourier sublayer applies a 2D Discrete Fourier Transform (DFT) to its input – one 1D DFT along the sequence dimension,  $\mathcal{F}_{\text{seq}}$ , and one 1D DFT along the hidden dimension,  $\mathcal{F}_h$ :

$$y = \Re(\mathcal{F}_{\text{seq}}(\mathcal{F}_h(x))). \quad (1)$$

Following (Lee-Thorp et al., 2021), we only keep the real part of the result.

The Hartley sublayer uses Equation (1) with the DFT replaced with the Discrete Hartley Transform,  $\mathcal{H}$ . The Hartley Transform, which transforms real input to real output, can be described in terms of the Fourier Transform:  $\mathcal{H} = \Re\{\mathcal{F}\} - \Im\{\mathcal{F}\}$ .<sup>5</sup> We compute the Fourier and Hartley transforms using the Fast Fourier Transform (FFT) (Cooley and Tukey, 1965; Frigo and Johnson, 2005).

In Equation (1), we multiply along both the sequence and hidden dimensions. Although the primary purpose of a mixing layer is to combine inputs along the sequence dimension, we follow Lee-Thorp et al. (2021) who empirically found that also mixing along the hidden dimension improved model quality.

### 3.3.2 Structured matrix projections

We explore structured matrices under the hypothesis that adding structure to the mixing basis, may improve the distribution of output representations.

<sup>5</sup>In the case of the Hartley Transform, we may drop the  $\Re$  from Equation (1).

We consider two parameterized, structured matrices: Toeplitz and circulant. A Toeplitz matrix is a matrix in which each diagonal is constant:

$$\mathcal{T} = \begin{bmatrix} a & b & c \\ d & a & b \\ e & d & a \end{bmatrix}. \quad (2)$$

A circulant matrix is a particular kind of Toeplitz matrix, in which all rows are composed of the same elements but rotated one element to the right relative to the preceding row:

$$\mathcal{C} = \begin{bmatrix} a & b & c \\ c & a & b \\ b & c & a \end{bmatrix}. \quad (3)$$

For both structured matrices, the weights  $a, b, \dots$  are learned. The corresponding mixing sublayer mixes along the sequence and hidden dimension. For example, for the Toeplitz case, we perform:

$$y = \mathcal{T}_{\text{seq}} \mathcal{T}_h x, \quad (4)$$

where  $\mathcal{T}_{\text{seq}}$  and  $\mathcal{T}_h$  denote Toeplitz matrices.<sup>6</sup>

### 3.3.3 Vanilla matrix projections

We also consider "unstructured", fully dense parameterized matrix projections:

$$\mathcal{L} = \begin{bmatrix} a & b & c \\ d & e & f \\ g & h & i \end{bmatrix}. \quad (5)$$

Following Lee-Thorp et al. (2021), we call the mixing sublayer arising from this case, the "Linear" sublayer. The Linear matrix sublayer performs the same FLOPS as the structured matrix sublayers (provided the FFT is *not* used), but is more flexible due to the increased number of matrix weights.

## 3.4 Implementation

We train and optimize our model on 8 V100 GPUs. Our ablations may yield slightly different speed-accuracy trade-offs on other accelerators (e.g. TPU), but we believe that our results are reasonably robust as almost all of our modifications boil down to accelerator friendly matrix multiplications.

<sup>6</sup>Circulant matrices can be diagonalized by the DFT, and hence matrix multiplications involving circulant matrices can be computed efficiently using the FFT (Davis, 1970). A Toeplitz matrix may be embedded in a circulant matrix to take advantage of the same FFT computation. In practice, we find that for the standard sequence lengths we consider (512), diagonalizing the computation is slower than direct matrix multiplications on both GPU and TPU.

In Section 4.2.2, we scale our model sizes up and down on TPUs and find that the same favorable efficiency trade-offs persist.

Our model uses JAX (Bradbury et al., 2018) in the Flax framework (Heek et al., 2020). Full source code will be made available online.<sup>7</sup>

## 4 Results

We train in the typical transfer learning setting (Devlin et al., 2019): Masked Language Modelling (MLM) and Next Sentence Prediction (NSP) pre-training, followed by fine-tuning. Our starting point is the BERT "Base" configuration (Devlin et al., 2019) and we follow BERT's pre-training setup with a few updates: (1) we pre-train on the much larger C4 dataset (Raffel et al., 2020); (2) we use a 32000 SentencePiece vocabulary model (Kudo and Richardson, 2018) trained on a 100 million sentence subset of C4; and (3) we use a smaller batch size of 64 (Devlin et al. (2019) uses 256). We use the a sequence length of 512 for all of pre-training. Experiments are run on 8 V100 GPU chips, except for the scaling experiments (Section 4.2.2) which are run on  $4 \times 4$  TPU v2 chips.

In Section 4.1, we optimize our model through a "coordinate descent" over model configurations. In Section 4.2.1, we then compare our optimized Sparse Mixer with BERT on GLUE (Wang et al., 2018) and SuperGLUE (Wang et al., 2019), over a broad set of training configurations, and also compare model vital statistics such as inference latency and FLOPS. We study the Pareto efficiency of Sparse Mixer models over a range of smaller and large model configurations in Section 4.2.2. Section 4.2.3, shows that, with minimal quality loss, the Sparse Mixer can be sped up even further. Finally, in Section 4.3, we compare Sparse Mixer with sparsified BERT models.

### 4.1 Coordinate descent

We follow a coordinate descent through our model configurations until we arrive at the final Sparse Mixer design. Given the large number of model hyperparameters to explore, we perform multiple parameter searches in parallel. For example, the model shape and MoE configurations are explored independently and then the most promising configurations from each program are combined. Because we are optimizing one model configuration coordi-

<sup>7</sup>We're still working on it, but it will soon be made available at [https://bit.ly/sparse\\_mixers](https://bit.ly/sparse_mixers)

nate at a time – some of which we perform in parallel – our manual gradient descent is pedagogical but potentially sub-optimal. It would be exciting to see future work expand both the coordinate space and jointly optimize multiple coordinates using Automated Machine Learning (AutoML) (Thornton et al., 2013; Liu et al., 2019a; Peng et al., 2020).

For our coordinate descent study, we only pre-train for  $500k$  steps, which we found to be reasonably indicative of model performance. Models are fine-tuned with the same batch size (64) on the Validation split of each respective GLUE task for 5 epochs and the best result for each task is selected from across three base learning rates (adapted from Devlin et al. (2019)):  $\{10^{-5}, 5 \cdot 10^{-5}, 10^{-4}\}$ . Our final model is pre-trained for longer and is evaluated on both GLUE and SuperGLUE for a broader set of training configurations. Given the reduced training setup, we view the GLUE results in our coordinate descent study as merely indicative of relative model improvements.

We prioritize efficiency (speed and accuracy), rather than simply accuracy. We use pre-training step speed as a proxy for model latency. And we use both average GLUE scores and pre-training accuracy as our accuracy metrics, rather than only relying up upstream pre-training performance, which can be misleading (Tay et al., 2021b). In particular, we generally rely on average GLUE accuracy as the primary metric, but fallback to MLM and NSP metrics when GLUE scores between model variants are similar. Full GLUE results for all coordinate descent experiment are provided in Appendix A.1.

#### 4.1.1 Mixing

**Mixing mechanisms.** We first compare the mixing mechanisms discussed in Section 2.2. For each mixing model, we replace *all* self-attention sublayers with the corresponding mixing sublayer. The results are shown in Table 1. The spectral models (Fourier and Hartley) perform the best on GLUE. The Linear model slightly under-performs the spectral models, while the structured mixing models (Circulant and Toeplitz) perform worst on GLUE. The pre-training metrics are a little more muddled, with the Hartley and Circulant models performing relatively well on MLM and the Linear model performing best on NSP. The spectral methods, efficiently implemented using FFTs, are the fastest.<sup>8</sup>

<sup>8</sup>There is some noise in the speed measurement, so we don't read too much into the small speed differences between the Fourier and Hartley models.

Table 1: Average accuracy metrics and median pre-training step speeds for mixing models. The "Fourier" model is identical to FNet (Lee-Thorp et al., 2021). Speed-ups relative to BERT (see Table 11) are shown in parentheses. The best metrics are highlighted in bold-face, while the second best metrics are underlined.

Model	Accuracy (%)			Speed (ms/batch)
	GLUE	MLM	NSP	
Fourier	<b>78.4</b>	55.7	75.4	<b>173 (1.75x)</b>
Hartley	<u>78.0</u>	<b>58.5</b>	74.9	<b>172 (1.77x)</b>
Circulant	75.1	<u>58.3</u>	75.6	200 (1.52x)
Toeplitz	76.5	57.7	<u>76.5</u>	<u>200 (1.52x)</u>
Linear	77.7	57.6	<b>77.4</b>	<u>200 (1.52x)</u>

Table 2: Metrics for hybrid attention-mixing models. Hartley- $k$  denotes a model with  $k$  self-attention sublayers and  $12 - k$  Hartley sublayers.

Model	Accuracy (%)			Speed (ms/batch)
	GLUE	MLM	NSP	
Hartley-0	78.0	58.5	74.9	<b>172 (1.76x)</b>
Hartley-1	78.0	51.9	75.3	<u>183 (1.66x)</u>
Hartley-2	81.1	61.3	79.8	<u>193 (1.57x)</u>
Hartley-3	77.9	50.3	76	204 (1.49x)
Hartley-4	82.7	62.6	81	216 (1.41x)
Hartley-6	82.9	63.5	81.2	234 (1.30x)
Linear-0	77.7	57.6	77.4	200 (1.51x)
Linear-1	78.1	62.5	78.3	208 (1.46x)
Linear-2	82.8	62.8	81	218 (1.40x)
Linear-3	82.8	63.3	81.6	226 (1.35x)
Linear-4	<u>83.4</u>	63.6	<u>81.7</u>	235 (1.29x)
Linear 6	<b>83.6</b>	<b>64</b>	<u>81.7</u>	251 (1.21x)

**Hybrid mixing-attention.** Lee-Thorp et al. (2021) observed that hybrid mixing-attention models outperform pure mixing models. With this in mind, we choose two strong candidates from Table 1, namely the Hartley and Linear mixing models, and replace a subset of the topmost mixing sublayers with self-attention. The results are summarized in Table 2.

Once we include self-attention, we see that the Linear model offers larger quality gains than the Hartley model. Even though the hybrid Hartley models are faster, an iso-speed comparison (e.g. Hartley-6 and Linear-4) still suggests that the hybrid Linear models are more efficient. Because our goal is to design a model that is faster than BERT but at least matches BERT quality, we opt to use the Linear-4 model.

We next proceed to determine where the 4 atten-

Table 3: Varying the self-attention sublayer placement within the Linear-4 model.

Layout	Accuracy (%)			Speed
	GLUE	MLM	NSP	(ms/batch)
BOTTOM	82	62.6	81	236 (1.29x)
MIDDLE	82.4	63.2	80.7	236 (1.29x)
MIXED	82.7	<b>63.6</b>	81.1	235 (1.29x)
TOP	<b>83.4</b>	<b>63.6</b>	<b>81.7</b>	235 (1.29x)

Table 4: Metrics for various intermediate MLP activation dimension,  $d_{ff}$ , sizes. Speed-ups relative to BERT (see Table 11) are shown in parentheses.

$d_{ff}$	Accuracy (%)			Speed
	GLUE	MLM	NSP	(ms/batch)
3072	83.4	<b>63.6</b>	<b>81.7</b>	235 (1.29x)
2560	83.2	<u>62.2</u>	<u>81.1</u>	208 (1.46x)
2048	<b>83.5</b>	62	81	189 (1.61x)
1024	82.9	60.7	80.6	<u>146 (2.09x)</u>
768	82.8	60.4	80.7	<b>135 (2.24x)</b>

tion sublayers should be placed within the model. In particular, we check whether it best to place the 4 self-attention sublayers at the TOP (final 4 layers), BOTTOM (first 4 layers), MIDDLE (middle 4 layers) or MIXED (every third layer). Table 3 shows that the TOP layout is best.

**Dead ends.** We tested two other mixing modifications that yielded no quality (or latency) gains: (1) adding a bias term to the mixing transformations, and (2) adding dropout during fine-tuning to the mixing sublayers.

#### 4.1.2 Model shape

All model shape experiments start from the same Base configuration as all were run in parallel.

**Intermediate and model dimensions.** In seeking a more efficient model, we attempt to slim our model down both by decreasing the intermediate

Table 5: Varying the model dimension,  $d_m$ . As in the Transformer, we set the model and embedding dimension to be equal. For the self-attention sublayers, we fix always fix the number of self-attention heads to  $d_m/64$ .

$d_m$	Accuracy (%)			Speed
	GLUE	MLM	NSP	(ms/batch)
768	<b>83.4</b>	<b>63.6</b>	<b>81.7</b>	235 (1.29x)
512	<u>83.0</u>	<u>62.5</u>	<u>80.9</u>	161 (1.89x)
256	80.7	58.9	78.4	<u>91 (3.34x)</u>
128	71.6	54	73.8	<b>58 (5.29x)</b>

Table 6: Varying the number of model layers. The results are for post-layer normalization, as in BERT. We obtained similar results for pre-layer normalization.

Layers	Accuracy (%)			Speed
	GLUE	MLM	NSP	(ms/batch)
6	82.3	62.4	80.9	<b>142 (2.14x)</b>
10	<u>83.6</u>	63.4	81.4	<u>201 (1.51x)</u>
12	83.4	63.6	<b>81.7</b>	235 (1.29x)
14	<b>83.8</b>	<b>64</b>	<u>81.6</u>	260 (1.17x)
18	<b>83.8</b>	<u>63.9</u>	81.5	320 (0.95x)

MLP activation dimension and the model dimension. For each coordinate, we find that there are cutoffs ( $d_{ff} = 2048$  and  $d_m = 512$ ) below which model quality drops drastically. We select these cutoffs as our optimal model shape values. It is in decreasing these two hyperparameters that we obtain the biggest speed-up in our model. However, there is a material degradation in quality that must be compensated by the increased capacity in the MoE sublayers in Section 4.1.3.

**Number of layers.** We also try varying the number of layers. We do not see quality gains beyond 14 layers. Because we plan to thin out our model (decrease  $d_{ff}$  and  $d_m$ ), we opt for slightly increasing the number of layers to 14.

#### 4.1.3 MoE

Our starting point for our MoE ablations is the Linear-4 model with every other dense MLP sublayer replaced by an MoE sublayer (6 MoE sublayers) and 16 experts in each MoE sublayer. We performed the MoE experiments in parallel to the model shape optimizations, so all MoE ablations are performed on a default Base sized model with 12 layers,  $d_{ff} = 3072$  and  $d_m = 768$ .

As observed by Zoph et al. (2022), we find that we must adjust the fine-tuning learning protocol to transfer the MLM pre-training gains downstream. In particular, our MoE encoder models benefit from larger base learning rates ( $\{10^{-4}, 5 \cdot 10^{-4}, 10^{-3}\}$ ) and larger dropout rates (0.2) for experts; see Appendix A.2 for a comparison of learning rates and expert dropout rates. For our final model comparison with BERT in Section 4.2, we consider a wide range of base learning rates for all models.<sup>9</sup>

**Routers.** Routing mechanisms are compared in Table 7. We use Experts Choose routing algorithm

<sup>9</sup>Consistent with (Zoph et al., 2022), we find that the larger base learning rates are not beneficial for the dense models.



Table 7: Accuracy and speed metrics for Top-1 Tokens Choose (TC) and Experts Choose (EC) routing. We found that increasing  $k > 1$  (number of selected experts) for Tokens Choose routing yielded no quality gains over  $k = 1$ .

Router	Accuracy (%)			Speed
	GLUE	MLM	NSP	(ms/batch)
TC	83.4	64	80.8	280 (1.09x)
EC	<b>83.5</b>	<b>64.6</b>	<b>81.2</b>	283 (1.08x)

going forward as it obtains slightly higher accuracy results and is simpler (no load balancing loss).

**MoE layers.** In Table 8, we vary the number of MoE sublayers and the layout of those layers within the model. As we increase the number of MoE layers, MLM accuracy improves, but these pre-training gains do not always lead to better GLUE performance. This was a general trend that we noted: with abundant pre-training data, more MoE layers, and therefore larger model capacity, leads to stronger MLM results; however, on smaller fine-tuning datasets, there may be insufficient training signal to utilize the increased model capacity downstream.<sup>10</sup> We opt for 4 MoE layers, which performs well on GLUE and slightly better than the 2 MoE sublayer model on the MLM task.

The results of MoE layout experiments are clearer – we opt to use the MIDDLE layout, placing all MoE sublayers in the middle layers of the model. Nevertheless, it is interesting to note that the TOP layout gives a big boost to MLM accuracy, but does not improve downstream GLUE accuracy. It is possible that the TOP layout would perform better on a downstream task with a larger dataset.

**Number of experts.** In Table 9, we increase the number of experts to increase the capacity of the model. As discussed in Section 3.2, we simultaneously decrease each expert’s capacity (the number of tokens it processes) to prevent FLOPS from growing. We suspect that, for a large number of experts, the training signal to an individual expert becomes too weak to facilitate effective training as each expert processes too small a slice of data. This is particularly apparent on downstream tasks where there are fewer training examples. Furthermore, for a large number of experts ( $\geq 64$ ), the computational cost of the routing assignment starts to become significant. Seeking a compromise be-

<sup>10</sup>This may be less of a concern for T5-style models (Raffel et al., 2020) as they are simultaneously fine-tuned on all GLUE or SuperGLUE tasks.

Table 8: Varying the number and layout of MoE sublayers. Layout definition: 6-BOTTOM (first 6 layers), 6-MIDDLE (middle 6 layers) or 6-MIXED (every odd layer), 6-MIXED\* (every even layer), and 6-TOP (final 6 layers).

Config	Accuracy (%)			Speed
	GLUE	MLM	NSP	(ms/batch)
2-MIXED	83.6	63.6	81.3	<b>246 (1.23x)</b>
4-MIXED	83.6	63.9	81.3	264 (1.15x)
6-MIXED	83.5	64.6	81.2	283 (1.08x)
12-MIXED	83.1	64.9	81.4	352 (0.86x)
6-BOTTOM	83.2	62.7	81.4	289 (1.05x)
6-MIDDLE	<b>83.9</b>	64	<b>81.7</b>	284 (1.08x)
6-MIXED	83.5	64.6	81.2	283 (1.08x)
6-MIXED*	83.2	64.8	81.6	292 (1.04x)
6-TOP	83.4	<b>65.4</b>	81.2	287 (1.06x)

Table 9: Increasing the number of experts. These experiments were run in parallel to those of Table 8 and therefore use the default 6-MIXED setup. Speed-ups relative to BERT (see Table 11) are shown in parentheses. Based on the speed slowdown for 64 experts and the relatively weak performance of 32 experts, we did not evaluate 64 experts on GLUE.

Experts	Accuracy (%)			Speed
	GLUE	MLM	NSP	(ms/batch)
8	83.3	64.1	81.2	<b>277 (1.10x)</b>
16	<b>83.5</b>	64.6	<u>81.2</u>	283 (1.08x)
32	83.3	<u>65.1</u>	<b>81.3</b>	292 (1.04x)
64	-	<b>65.4</b>	80.9	327 (0.93x)

tween quality and speed, we ultimately opt to use 16 experts.<sup>11</sup>

**Expert size.** The number of parameters in each expert can be controlled by varying its intermediate activation dimension,  $d_{ff}$ . If we can maintain accuracy while decreasing the size of each expert, that will speed up our model. On the other hand, if we can achieve large accuracy gains by increasing the size of experts, we can potentially use that to offset shrinking the rest of the model; for example, by constructing a "thin", fast model with only a few "heavy", high capacity MoE layers. In Table 10, we see that neither of these scenarios plays out cleanly: (1) Using smaller experts ( $d_{ff} = 1536$ ) yields only a small accuracy drop, but little speed benefit. (2) And, as was the case for increasing the number of MoE sublayers and the number of

<sup>11</sup>The optimal experts will vary based on hardware and the training dataset size.

Table 10: Varying the size of experts by varying each expert’s intermediate activation dimension,  $d_{ff}$ . These experiments were run in parallel to those of Table 8 and therefore use the default 6-MIXED setup.

$d_{ff}$	Accuracy (%)			Speed (ms/batch)
	GLUE	MLM	NSP	
1536	83.4	64	81.1	<b>274 (1.11x)</b>
3072	<b>83.5</b>	64.6	81.2	283 (1.08x)
6144	83.3	<u>65.3</u>	<u>81.5</u>	305 (1.00x)
12288	83.1	<b>65.9</b>	<b>81.7</b>	350 (0.87x)

experts, increasing expert size increases MLM accuracy, but the results do not translate downstream to GLUE. For simplicity, we opt to keep the expert  $d_{ff}$  the same size as the dense  $d_{ff}$  (optimized in Section 4.1.2).

**Dead ends.** (1) Changing the expert nonlinearity from GELU to RELU had little effect on downstream performance. Changing the nonlinearity to GEGLU (GELU Gated Linear Units) (Shazeer, 2020) only slowed down the model.<sup>12</sup> (2) Although the router z-loss had little effect on model performance, we included it for potential stability benefits. (2) Fedus et al. (2022) recommend using a smaller scaled weight initialization to provide stability to MoE models, especially in larger configurations. However, we obtained the best results with BERT’s default kernel initialization.

## 4.2 Sparse Mixer

Putting the preceding results together, we arrive at the Sparse Mixer model:

$$\begin{aligned}
 \text{Shape} &: 14 \text{ layers, } 512 d_m, 2056 d_{ff}; \\
 \text{Sparse} &: 4 \text{ MIDDLE MoE, } 16 \text{ experts, } \quad (6) \\
 & \quad 2056 d_{ff}, \text{ EC routing, } 1.0 cf; \\
 \text{Mixer} &: \text{Linear, } 4 \text{ TOP Attention layers.}
 \end{aligned}$$

### 4.2.1 Full training comparison with BERT

The Sparse Mixer is pre-trained on C4 for the full 1M steps (with batch size 64) and is evaluated, alongside BERT, on both GLUE and SuperGLUE for a larger range of fine-tuning batch sizes (16, 32, and 64) and base learning rates ( $\{10^{-5}, 5 \cdot 10^{-5}, 10^{-4}, 5 \cdot 10^{-4}, 10^{-3}\}$ ). The best results across all learning rates (for each task) and batch sizes (for all tasks) are shown in Table 12

<sup>12</sup>An important limitation of our GEGLU investigation is that we did not simultaneously shrink the intermediate activation dimension to account for the extra activation function, as in (Shazeer, 2020; Narang et al., 2021).

Table 11: Model computational characteristics, measured by GFLOPS per example and number of model parameters ("size" in millions); and run speeds, measured by inference speed per example and pre-training step speed per example. We use the abbreviations SM for Sparse Mixer and FSM for Fast Sparse Mixer, which is introduced in Section 4.2.3. Although they are "thinner" (smaller model dimension), the Sparse Mixer models overall have more parameters than BERT because of their MoE sublayers.

Model	GFLOPS (/ex)	Size (M)	Inference (ms/ex)	Training (ms/ex)
BERT	102	112	1.34	4.75
SM	73	180	0.84 (1.61x)	2.87 (1.65x)
FSM	<b>60</b>	180	<b>0.68 (1.98x)</b>	<b>2.51 (1.89x)</b>

(GLUE) and Table 13 (SuperGLUE); see Appendix A.1 for results for all batch sizes.<sup>13</sup> Note that these results may be slightly different to the original BERT results (Devlin et al., 2019) as our models see fewer tokens during pre-training because of the smaller batch size (64 vs 256).

GLUE scores between BERT and Sparse Mixer are very similar. Sparse Mixer and BERT diverge a little more on SuperGLUE, where the Sparse Mixer performs particularly well on the CB task, but underperforms BERT on the multi-label MultiRC and ReCoRD tasks. Sparse Mixer also performs better on COPA, although both models generally perform quite poorly.

### 4.2.2 Scaling the Sparse Mixer

Tables 11-13 indicate that the Sparse Mixer is more efficient than BERT in the Base configuration. What about for smaller or larger model configurations? In Figure 3, we compare BERT and Sparse Mixer across a selection of model sizes. We use MLM accuracy as a proxy for model accuracy and pre-training step speed as a proxy for overall model speed. Table 11 indicates that pre-training step speed is a good proxy for inference speed. Although MLM accuracy is a less ideal benchmark for downstream accuracy, the results of Section 4.1 suggest that it is at least indicative. We construct an analogous speed-accuracy figure for NSP accuracy in Figure 4 in Appendix A.3.

These caveats aside, Figure 3 suggests that Sparse Mixer’s favorable speed and accuracy extends to other model sizes. In particular, the Sparse Mixer family of models dominates the efficiency

<sup>13</sup>Following Devlin et al. (2019), we omit the WNLI task.

Table 12: GLUE results on the *Validation* split. We report F1/accuracy scores for QQP and MRPC, Spearman correlations for STS-B and accuracy scores for all other tasks. The MNLI accuracy metrics are reported by the match/mismatch splits.

Model	MNLI	QQP	QNLI	SST-2	CoLA	STS-B	MRPC	RTE	Avg.
BERT	<b>81.3 / 81.8</b>	86.7 / 90.3	88.9	<b>91.1</b>	77.6	87.3	<b>90.5 / 86.8</b>	69.7	84.7
Sparse Mixer	80.7 / 81	<b>87.1 / 90.5</b>	<b>89.1</b>	90.9	<b>79</b>	<b>88.1</b>	90.4 / 86.3	<b>72.2</b>	<b>85.0</b>

Table 13: SuperGLUE *Validation* results. We report macro-F1 scores for CB, micro-F1/exact match scores for MultiRC, F1/exact match scores for ReCoRD, and accuracy scores for all other tasks.

Model	BoolQ	CB	COPA	MultiRC	ReCoRD	RTE	WiC	Avg.
BERT	<b>74.6</b>	86.4 / 85.7	58	<b>74.1 / 26.2</b>	<b>68.6 / 52.2</b>	<b>65</b>	65.7	65.7
Sparse Mixer	74.4	<b>93.3 / 92.9</b>	<b>62</b>	72.4 / 22.5	65.9 / 49.2	64.6	<b>66.5</b>	<b>66.4</b>

Table 14: Faster Sparse Mixers. The default Sparse Mixer uses a capacity factor ( $cf$ ) of 1 and a group size ( $g$ ) of 4096. Several less favorable values are omitted:  $cf = 0.75$  was slower than  $cf = 0.5$  and yielded minimal quality gains;  $cf = 0.5$  with  $g = 2048$  or  $g = 1024$ , and  $cf = 0.75$  with  $g = 1024$ , yielded significant quality dips on SuperGLUE.

Model	Accuracy (%)		Speed (ms/batch)
	GLUE	SuperGLUE	
BERT	<u>84.7</u>	<u>65.7</u>	304
SM	<b>85.0</b>	<b>66.4</b>	184 (1.65x)
w/ $cf=0.5$	<u>84.7</u>	65.6	<b>161 (1.89x)</b>
w/ $g=2048$	84.5	65.1	173 (1.75x)
w/ $g=1024$	84.1	64.0	167 (1.82x)
w/ $cf=0.75$	84.3	65.2	<u>165 (1.84x)</u>
+ $g=2048$			

frontier across all model sizes considered.<sup>14</sup>

#### 4.2.3 Trading accuracy for more speed

If we are willing to sacrifice 1% accuracy, we can design an even faster Sparse Mixer. Rather than revisiting many of our decisions in Sections 4.1, in Table 14, we turn to two simpler knobs, introduced in Section 3.2, that we can vary in the Sparse Mixer: expert capacity and token group size. By decreasing either of these, we speed up the MoE sublayers and the model overall.

Decreasing the capacity factor offers big speed-ups for a limited quality degradation: For a minor (0.15%) accuracy drop on SuperGLUE relative to

<sup>14</sup>Figure 3 omits BERT-Large, which was too unstable to train in our training setup. This may be because we use a faster learning rate warm-up (2.5k steps) when training for 250k steps than the original BERT paper, although the authors did also note stability concerns. However, we do include an 18 layer BERT model that sits between Base and Large; see Table 20 for details.

BERT, a Sparse Mixer with capacity factor of 0.5 trains 89% faster and runs inference 98% faster (Table 11). We name this variant of the model the Fast Sparse Mixer. It is possible that the minimal accuracy drop for the decreased capacity factor could be mitigated by training with default capacity factor (1.), and then use a smaller factor during inference, although the mismatch may yield unexpected results during inference. Decreasing the group size appears to be less effective as it leads to larger quality drops.

#### 4.3 Sparse BERT

A natural baseline omitted in the preceding analysis is a "sparse BERT" model, wherein the only change we make to BERT is to replace a subset of the dense MLP sublayers with MoE sublayers. This would result in a slower model, but could potentially yield quality gains. However, the real challenge turns out to be the stability of such a model.

In Table 15, we compare the accuracy, speed and stability of MoE variants of BERT. We find that only the fully sparsified BERT model (BERT-12) had any stable runs in our experiments. Unfortunately, this model is both slow and significantly underperforms (dense) BERT on SuperGLUE. It is possible that with more trials, we will eventually find a BERT-4 model that is also trained successfully, but working with a model which trains robustly only < 25% of the time is not practical.<sup>15</sup> Stability aside, even if the sparse BERT models could be made more stable, they would inevitably be slower than BERT.

On the other hand, Table 15 highlights that the Sparse Mixer is very stable. We hypothesize that

<sup>15</sup>We also tried increasing the batch size from 64 to 256, but that did not improve the stability of the sparse BERT models.

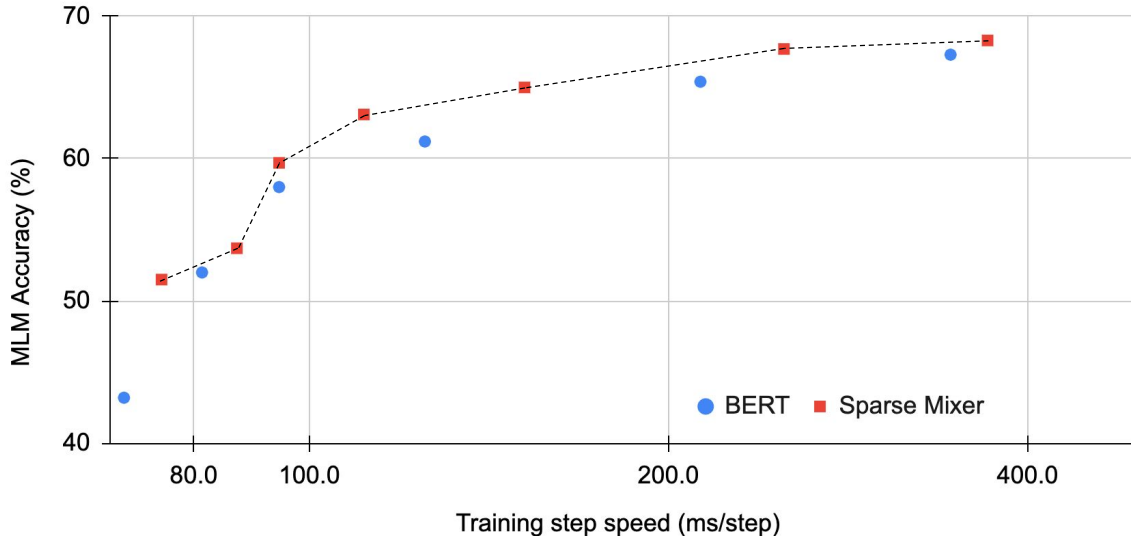


Figure 3: Pre-training Speed-accuracy trade-offs for Sparse Mixer and BERT. The corresponding model configurations are shown in Table 20 in Appendix A.3. The dashed line shows the Pareto efficiency frontier, indicating the best trade-offs. All models are trained on  $4 \times 4$  TPU v2 chips. To better utilize the increased number of devices, we use a larger batch size of 256 but train for fewer (250k) steps.

Table 15: Stability of BERT, sparse BERT and Sparse Mixer (SM). BERT- $k$  denotes a BERT model with  $k$  MoE sublayers.

Model	Stable Runs	Accuracy (%)		Speed (ms/batch)
		GLUE	S.GLUE	
BERT	3/4	84.7	65.7	304
SM	<b>4/4</b>	<b>85.0</b>	<b>66.4</b>	<b>184 (1.65x)</b>
BERT-4	0/4	-	-	-
BERT-12	1/4	84.1	60.9	426 (0.71x)

this stability is due to replacing the majority of self-attention sublayers with Linear mixing sublayers, which constrains the sublayers to a less variable mixing basis.

## 5 Conclusions

We have demonstrated that mixing transformations and MoE play well together. Utilizing MoE for capacity and mixing for speed and stability, we introduced the Sparse Mixer encoder model – a model that slightly ( $< 1\%$ ) *outperforms* BERT on GLUE and SuperGLUE, but more importantly trains 65% faster and runs inference 61% faster. We also presented a faster variant, Fast Sparse Mixer, that marginally ( $< 0.2\%$ ) *under-performs* BERT on SuperGLUE, but trains and runs nearly twice as fast: 89% faster training and 98% faster inference. We justified the design of these two models by care-

fully ablating through various mixing mechanisms, MoE configurations, and model hyperparameters. The Sparse Mixer overcomes the speed and stability concerns of MoE models and offers the prospect of serving sparse student models.

Throughout this work we have restricted our focus to encoders. In future work, we plan to investigate porting the recipes outlined in this paper to encoder-decoder models (Raffel et al., 2020). Sparse mixer encoder-decoder (and decoder-only) models are, in principle, straightforward extensions: Linear decoders can be designed by “causally” masking the Linear matrix and encoder-decoder mixing can also be designed with careful masking. However, we suspect that parts of the coordinate descent program will need to be repeated. For example, evidence suggests that cross-attention may be crucial to performance (You et al., 2020) of Transformer-like encoder-decoder models. We do remark that the sparse mixer encoder could be used as a drop in replacement in a Transformer as other works have successfully demonstrated; see, for example, (Zaheer et al., 2020; Guo et al., 2021).

There are also a number of orthogonal future directions that could be adapted to potentially improve the training regime of the Sparse Mixer, such as training for much longer as for RoBERTa (Liu et al., 2019b) or using the ELECTRA generator-discriminator training setup (Clark et al., 2020).



## Acknowledgements

We would like to give a big thanks to Parker Schuh for critical help with the Mixture-of-Experts implementation. We also thank Santiago Ontañón for many helpful brainstorming sessions around the design and evaluation of the Sparse Mixer model.

## References

- Mikel Artetxe, Shruti Bhosale, Naman Goyal, Todor Mihaylov, Myle Ott, Sam Shleifer, Xi Victoria Lin, Jingfei Du, Srinivasan Iyer, Ramakanth Pasunuru, Giri Anantharaman, Xian Li, Shuohui Chen, Halil Akin, Mandeep Baines, Louis Martin, Xing Zhou, Punit Singh Koura, Brian O’Horo, Jeff Wang, Luke Zettlemoyer, Mona T. Diab, Zornitsa Kozareva, and Ves Stoyanov. 2021. [Efficient large scale language modeling with mixtures of experts](#). *CoRR*, abs/2112.10684.
- James Bradbury, Roy Frostig, Peter Hawkins, Matthew James Johnson, Chris Leary, Dougal Maclaurin, George Necula, Adam Paszke, Jake VanderPlas, Skye Wanderman-Milne, and Qiao Zhang. 2018. [JAX: composable transformations of Python+NumPy programs](#).
- Jane Bromley, Isabelle Guyon, Yann LeCun, Eduard Säcker, and Roopak Shah. 1993. Signature verification using a "siamese" time delay neural network. *Advances in neural information processing systems*, 6.
- Tom Brown, Benjamin Mann, Nick Ryder, Melanie Subbiah, Jared D Kaplan, Prafulla Dhariwal, Arvind Neelakantan, Pranav Shyam, Girish Sastry, Amanda Askell, Sandhini Agarwal, Ariel Herbert-Voss, Gretchen Krueger, Tom Henighan, Rewon Child, Aditya Ramesh, Daniel Ziegler, Jeffrey Wu, Clemens Winter, Chris Hesse, Mark Chen, Eric Sigler, Mateusz Litwin, Scott Gray, Benjamin Chess, Jack Clark, Christopher Berner, Sam McCandlish, Alec Radford, Ilya Sutskever, and Dario Amodei. 2020. [Language models are few-shot learners](#). In *Advances in Neural Information Processing Systems*, volume 33, pages 1877–1901. Curran Associates, Inc.
- Aidan Clark, Diego de Las Casas, Aurelia Guy, Arthur Mensch, Michela Paganini, Jordan Hoffmann, Bogdan Damoc, Blake A. Hechtman, Trevor Cai, Sebastian Borgeaud, George van den Driessche, Eliza Rutherford, Tom Hennigan, Matthew Johnson, Katie Millican, Albin Cassirer, Chris Jones, Elena Buchatskaya, David Budden, Laurent Sifre, Simon Osindero, Oriol Vinyals, Jack W. Rae, Erich Elsen, Koray Kavukcuoglu, and Karen Simonyan. 2022. [Unified scaling laws for routed language models](#). *CoRR*, abs/2202.01169.
- Kevin Clark, Minh-Thang Luong, Quoc V. Le, and Christopher D. Manning. 2020. [ELECTRA: pre-training text encoders as discriminators rather than generators](#). In *8th International Conference on Learning Representations, ICLR 2020, Addis Ababa, Ethiopia, April 26-30, 2020*. OpenReview.net.
- James W Cooley and John W Tukey. 1965. An algorithm for the machine calculation of complex fourier series. *Mathematics of computation*, 19(90):297–301.
- Philip J Davis. 1970. *Circulant matrices*. Wiley, New York.
- Jacob Devlin, Ming-Wei Chang, Kenton Lee, and Kristina Toutanova. 2019. [BERT: Pre-training of deep bidirectional transformers for language understanding](#). In *Proceedings of the 2019 Conference of the North American Chapter of the Association for Computational Linguistics: Human Language Technologies, Volume 1 (Long and Short Papers)*, pages 4171–4186, Minneapolis, Minnesota. Association for Computational Linguistics.
- William Fedus, Barret Zoph, and Noam Shazeer. 2022. [Switch transformers: Scaling to trillion parameter models with simple and efficient sparsity](#). *Journal of Machine Learning Research*, 23(120):1–39.
- Matteo Frigo and Steven G Johnson. 2005. The design and implementation of fftw3. *Proceedings of the IEEE*, 93(2):216–231.
- Mandy Guo, Joshua Ainslie, David Uthus, Santiago Ontanon, Jianmo Ni, Yun-Hsuan Sung, and Yinfei Yang. 2021. [Long5: Efficient text-to-text transformer for long sequences](#). *arXiv preprint arXiv:2112.07916*.
- Jonathan Heek, Anselm Levskaya, Avital Oliver, Marvin Ritter, Bertrand Rondepierre, Andreas Steiner, and Marc van Zee. 2020. [Flax: A neural network library and ecosystem for JAX](#).
- Robert A Jacobs, Michael I Jordan, Steven J Nowlan, and Geoffrey E Hinton. 1991. Adaptive mixtures of local experts. *Neural computation*, 3(1):79–87.
- Sebastian Jaszczur, Aakanksha Chowdhery, Afroz Mohiuddin, Lukasz Kaiser, Wojciech Gajewski, Henryk Michalewski, and Jonni Kanerva. 2021. [Sparse is enough in scaling transformers](#). In *Advances in Neural Information Processing Systems 34: Annual Conference on Neural Information Processing Systems 2021, NeurIPS 2021, December 6-14, 2021, virtual*, pages 9895–9907.
- Michael I Jordan and Robert A Jacobs. 1994. Hierarchical mixtures of experts and the em algorithm. *Neural computation*, 6(2):181–214.
- Jared Kaplan, Sam McCandlish, Tom Henighan, Tom B Brown, Benjamin Chess, Rewon Child, Scott Gray, Alec Radford, Jeffrey Wu, and Dario Amodei. 2020. [Scaling laws for neural language models](#). *arXiv preprint arXiv:2001.08361*.

- Vladimir Karpukhin, Barlas Oğuz, Sewon Min, Patrick Lewis, Ledell Wu, Sergey Edunov, Danqi Chen, and Wen-tau Yih. 2020. Dense passage retrieval for open-domain question answering. *arXiv preprint arXiv:2004.04906*.
- Taku Kudo and John Richardson. 2018. [SentencePiece: A simple and language independent subword tokenizer and detokenizer for neural text processing](#). In *Proceedings of the 2018 Conference on Empirical Methods in Natural Language Processing: System Demonstrations*, pages 66–71, Brussels, Belgium. Association for Computational Linguistics.
- Guillaume Lample, Alexandre Sablayrolles, Marc’Aurelio Ranzato, Ludovic Denoyer, and Hervé Jégou. 2019. Large memory layers with product keys. *Advances in Neural Information Processing Systems*, 32.
- James Lee-Thorp, Joshua Ainslie, Ilya Eckstein, and Santiago Ontanon. 2021. Fnet: Mixing tokens with fourier transforms. *arXiv preprint arXiv:2105.03824*.
- Dmitry Lepikhin, HyoukJoong Lee, Yuanzhong Xu, Dehao Chen, Orhan Firat, Yanping Huang, Maxim Krikun, Noam Shazeer, and Zhifeng Chen. 2021. [Gshard: Scaling giant models with conditional computation and automatic sharding](#). In *9th International Conference on Learning Representations, ICLR 2021, Virtual Event, Austria, May 3-7, 2021*.
- Mike Lewis, Shruti Bhosale, Tim Dettmers, Naman Goyal, and Luke Zettlemoyer. 2021. [BASE layers: Simplifying training of large, sparse models](#). In *Proceedings of the 38th International Conference on Machine Learning, ICML 2021, 18-24 July 2021, Virtual Event*, volume 139 of *Proceedings of Machine Learning Research*, pages 6265–6274. PMLR.
- Hanxiao Liu, Karen Simonyan, and Yiming Yang. 2019a. [DARTS: differentiable architecture search](#). In *7th International Conference on Learning Representations, ICLR 2019, New Orleans, LA, USA, May 6-9, 2019*. OpenReview.net.
- Yinhan Liu, Myle Ott, Naman Goyal, Jingfei Du, Mandar Joshi, Danqi Chen, Omer Levy, Mike Lewis, Luke Zettlemoyer, and Veselin Stoyanov. 2019b. [Roberta: A robustly optimized BERT pretraining approach](#). *CoRR*, abs/1907.11692.
- Sharan Narang, Hyung Won Chung, Yi Tay, Liam Fedus, Thibault Fevry, Michael Matena, Karishma Malkan, Noah Fiedel, Noam Shazeer, Zhenzhong Lan, Yanqi Zhou, Wei Li, Nan Ding, Jake Marcus, Adam Roberts, and Colin Raffel. 2021. [Do transformer modifications transfer across implementations and applications?](#) In *Proceedings of the 2021 Conference on Empirical Methods in Natural Language Processing*, pages 5758–5773. Association for Computational Linguistics.
- Daiyi Peng, Xuanyi Dong, Esteban Real, Mingxing Tan, Yifeng Lu, Gabriel Bender, Hanxiao Liu, Adam Kraft, Chen Liang, and Quoc Le. 2020. Pyglove: Symbolic programming for automated machine learning. *Advances in Neural Information Processing Systems*, 33:96–108.
- Colin Raffel, Noam Shazeer, Adam Roberts, Katherine Lee, Sharan Narang, Michael Matena, Yanqi Zhou, Wei Li, and Peter J Liu. 2020. Exploring the limits of transfer learning with a unified text-to-text transformer. *Journal of Machine Learning Research*, 21:1–67.
- Carlos Riquelme, Joan Puigcerver, Basil Mustafa, Maxim Neumann, Rodolphe Jenatton, André Susano Pinto, Daniel Keysers, and Neil Houlsby. 2021. Scaling vision with sparse mixture of experts. *Advances in Neural Information Processing Systems*, 34.
- Stephen Roller, Sainbayar Sukhbaatar, Arthur Szlam, and Jason Weston. 2021. [Hash layers for large sparse models](#). In *Advances in Neural Information Processing Systems 34: Annual Conference on Neural Information Processing Systems 2021, NeurIPS 2021, December 6-14, 2021, virtual*, pages 17555–17566.
- Noam Shazeer. 2020. Glu variants improve transformer. *arXiv preprint arXiv:2002.05202*.
- Noam Shazeer, Azalia Mirhoseini, Krzysztof Maziarz, Andy Davis, Quoc V. Le, Geoffrey E. Hinton, and Jeff Dean. 2017. [Outrageously large neural networks: The sparsely-gated mixture-of-experts layer](#). In *5th International Conference on Learning Representations, ICLR 2017, Toulon, France, April 24-26, 2017, Conference Track Proceedings*. OpenReview.net.
- Sainbayar Sukhbaatar, Jason Weston, Rob Fergus, et al. 2015. End-to-end memory networks. *Advances in neural information processing systems*, 28.
- Yi Tay, Dara Bahri, Donald Metzler, Da-Cheng Juan, Zhe Zhao, and Che Zheng. 2020. Synthesizer: Rethinking self-attention in transformer models. *arXiv preprint arXiv:2005.00743*.
- Yi Tay, Mostafa Dehghani, Samira Abnar, Yikang Shen, Dara Bahri, Philip Pham, Jinfeng Rao, Liu Yang, Sebastian Ruder, and Donald Metzler. 2021a. [Long range arena : A benchmark for efficient transformers](#). In *9th International Conference on Learning Representations, ICLR 2021, Virtual Event, Austria, May 3-7, 2021*.
- Yi Tay, Mostafa Dehghani, Jinfeng Rao, William Fedus, Samira Abnar, Hyung Won Chung, Sharan Narang, Dani Yogatama, Ashish Vaswani, and Donald Metzler. 2021b. Scale efficiently: Insights from pre-training and fine-tuning transformers. *arXiv preprint arXiv:2109.10686*.

- Chris Thornton, Frank Hutter, Holger H Hoos, and Kevin Leyton-Brown. 2013. Auto-weka: Combined selection and hyperparameter optimization of classification algorithms. In *Proceedings of the 19th ACM SIGKDD international conference on Knowledge discovery and data mining*, pages 847–855.
- Ilya O Tolstikhin, Neil Houlsby, Alexander Kolesnikov, Lucas Beyer, Xiaohua Zhai, Thomas Unterthiner, Jessica Yung, Andreas Steiner, Daniel Keysers, Jakob Uszkoreit, et al. 2021. Mlp-mixer: An all-mlp architecture for vision. *Advances in Neural Information Processing Systems*, 34.
- Ashish Vaswani, Noam Shazeer, Niki Parmar, Jakob Uszkoreit, Llion Jones, Aidan N Gomez, Łukasz Kaiser, and Illia Polosukhin. 2017. Attention is all you need. *Advances in neural information processing systems*, 30.
- Alex Wang, Yada Pruksachatkun, Nikita Nangia, Amanpreet Singh, Julian Michael, Felix Hill, Omer Levy, and Samuel Bowman. 2019. Superglue: A stickier benchmark for general-purpose language understanding systems. *Advances in neural information processing systems*, 32.
- Alex Wang, Amanpreet Singh, Julian Michael, Felix Hill, Omer Levy, and Samuel Bowman. 2018. [GLUE: A multi-task benchmark and analysis platform for natural language understanding](#). In *Proceedings of the 2018 EMNLP Workshop BlackboxNLP: Analyzing and Interpreting Neural Networks for NLP*, pages 353–355, Brussels, Belgium. Association for Computational Linguistics.
- Jason Weston, Sumit Chopra, and Antoine Bordes. 2015. [Memory networks](#). In *3rd International Conference on Learning Representations, ICLR 2015, San Diego, CA, USA, May 7-9, 2015, Conference Track Proceedings*.
- Weiqiu You, Simeng Sun, and Mohit Iyyer. 2020. [Hard-coded Gaussian attention for neural machine translation](#). In *Proceedings of the 58th Annual Meeting of the Association for Computational Linguistics*, pages 7689–7700. Association for Computational Linguistics.
- Manzil Zaheer, Guru Guruganesh, Kumar Avinava Dubey, Joshua Ainslie, Chris Alberti, Santiago Ontanon, Philip Pham, Anirudh Ravula, Qifan Wang, Li Yang, et al. 2020. Big bird: Transformers for longer sequences. *Advances in Neural Information Processing Systems*, 33:17283–17297.
- Yanqi Zhou, Tao Lei, Hanxiao Liu, Nan Du, Yanping Huang, Vincent Y. Zhao, Andrew M. Dai, Zhifeng Chen, Quoc Le, and James Laudon. 2022. [Mixture-of-experts with expert choice routing](#). *CoRR*, abs/2202.09368.
- Barret Zoph, Irwan Bello, Sameer Kumar, Nan Du, Yanping Huang, Jeff Dean, Noam Shazeer, and William Fedus. 2022. Designing effective sparse expert models. *arXiv preprint arXiv:2202.08906*.

## A Appendices

### A.1 Full GLUE and SuperGLUE results

Table 16 contains the full GLUE results for all of the coordinate descent experiments summarized in Section 4.1. Tables 17 and 18 contain the full results for GLUE and SuperGLUE, respectively, across all fine-tuning batch sizes, for the final model results tabulated in Sections 4.2-4.3.

### A.2 Optimizing fine-tuning protocols for MoE models

In Table 19, we compare GLUE results for different fine-tuning learning protocols. Consistent with (Zoph et al., 2022), we find that fine-tuning results are improved with an increased expert dropout (0.2) and larger base learning rates. Increasing the capacity factor,  $cf$ , yields quality gains but slows down the model. We did not find benefits from freezing different parts of the model during fine-tuning.

For MoE models in the main text, we always use an expert dropout of 0.2 during fine-tuning. Similarly, we use the larger base learning rates during the coordinate descent program (Section 4.1). However, when comparing Sparse Mixer with BERT (Section 4.2) we use a wider range of learning rates for both models.

### A.3 Speed-accuracy plots

Figure 4 shows the NSP-accuracy equivalent of the MLM-accuracy based efficiency plot in Figure 3.

Table 20 gives the model configurations that were used to construct Figure 3 (main text) and Figure 4 (Appendix A.3). In configuring the Sparse Mixer model sizes, we tried to roughly hew to the proportions in the Base model.

Table 16: Full GLUE results (*Validation* split) for all coordinate descent experiments. See the corresponding table for descriptions of each configuration. For dense models (Tables 1-6), we report the best scores across  $\{10^{-5}, 5 \cdot 10^{-5}, 10^{-4}\}$  base learning rates, while for MoE models (Tables 7-10), we use  $\{10^{-4}, 5 \cdot 10^{-4}, 10^{-3}\}$ . We report F1/accuracy scores for QQP and MRPC, Spearman correlations for STS-B and accuracy scores for all other tasks. The MNLI accuracy metrics are reported by the match/mismatch splits. The top two average scores for each experiment set are boldfaced/underlined.

Table	Model	MNLI	QQP	QNLI	SST-2	CoLA	STS-B	MRPC	RTE	Avg.
1	Fourier	74.5 / 75.6	84.3 / 88.3	82.2	88.5	69.6	80.2	83.5 / 73.8	62.1	<b>78.4</b>
	Hartley	75 / 75.7	84.4 / 88.1	82.6	87.7	69.4	80.9	82.2 / 72.1	59.9	<u>78.0</u>
	Circulant	69.7 / 70.9	83.3 / 87.6	76	89.2	76.1	56.1	82.7 / 71.8	62.8	75.1
	Toeplitz	73.2 / 73.5	84.2 / 88.3	78.1	88.6	73	66.1	82.6 / 71.6	62.8	76.5
	Linear	73.4 / 74.3	84.3 / 88.2	80.2	89.6	74.6	68.2	83.5 / 75.2	63.5	77.7
2	Hartley-0	75 / 75.7	84.4 / 88.1	82.6	87.7	69.4	80.9	82.2 / 72.1	59.9	78.0
	Hartley-1	72.7 / 73.6	83.9 / 87.8	82.1	86.8	71.1	79.5	82.8 / 75.7	62.1	78.0
	Hartley-2	79.5 / 78.3	86 / 89.7	86.2	89.3	74	85.7	84.6 / 76.7	62.1	81.1
	Hartley-3	74.2 / 75	83.5 / 87.9	81.9	88.8	70.4	78.3	83.1 / 73.3	61	77.9
	Hartley-4	79 / 80.2	86.7 / 90.1	87.2	89.9	75.2	86.1	87.5 / 82.4	65	82.7
	Hartley-6	80 / 81	86.7 / 90.2	88	90.7	75.3	86.5	87.3 / 81.9	64.6	82.9
	Linear-0	73.4 / 74.3	84.3 / 88.2	80.2	89.6	74.6	68.2	83.5 / 75.2	63.5	77.7
	Linear-1	74.4 / 74.9	84.9 / 88.8	81.8	91.4	78	69	83.4 / 73	59.9	78.1
	Linear-2	80.1 / 80.5	87 / 90.3	87.6	90	78.2	86.7	85.3 / 78.2	66.8	82.8
	Linear-3	80.2 / 81	87 / 90.4	87.3	90.5	77.9	87.8	84.7 / 78.4	66.1	82.8
	Linear-4	80.4 / 81.2	87.2 / 90.4	88	91.3	76.7	87.4	87.2 / 81.6	65.7	<u>83.4</u>
	Linear-6	80.7 / 81.6	87.3 / 90.6	87.8	90.5	78.2	87.2	88.7 / 83.6	63.9	<b>83.6</b>
	3	BOTTOM	79.1 / 79.6	86.8 / 90.3	86.2	90.7	73.2	85.5	87.5 / 82.1	61
MIDDLE		80 / 80.3	86.7 / 90.3	86.5	89.2	72.2	86.3	88.3 / 83.1	63.5	82.4
MIXED		79.5 / 80.3	87.1 / 90.5	87.6	90.7	75	85	87.1 / 82.1	64.6	82.7
TOP		80.4 / 81.2	87.2 / 90.4	88	91.3	76.7	87.4	87.2 / 81.6	65.7	83.4
4	$d_{ff}=3072$	80.4 / 81.2	87.2 / 90.4	88	91.3	76.7	87.4	87.2 / 81.6	65.7	<u>83.4</u>
	$d_{ff}=2560$	80.3 / 81.5	87.2 / 90.5	88.3	91.6	77.8	86.9	85.5 / 79.2	66.1	83.2
	$d_{ff}=2048$	80.4 / 81.1	87.1 / 90.5	87.7	91.3	76.6	87	87.8 / 82.4	66.8	<b>83.5</b>
	$d_{ff}=1024$	79.9 / 80.8	87 / 90.3	87.3	90	76.3	87.4	87.7 / 81.9	62.8	82.9
	$d_{ff}=768$	80.1 / 81.1	86.7 / 90.2	87.4	89.7	75.7	86.6	87.7 / 82.6	62.8	82.8
5	$d_m=768$	80.4 / 81.2	87.2 / 90.4	88	91.3	76.7	87.4	87.2 / 81.6	65.7	<b>83.4</b>
	$d_m=512$	80.1 / 80.9	86.6 / 90.1	87.4	90.8	77	87.2	86.3 / 80.1	66.4	<u>83.0</u>
	$d_m=256$	77.9 / 78.5	84.4 / 88.1	85.2	89.8	73.9	83.8	84.5 / 76	66.1	80.7
	$d_m=128$	74.9 / 75.9	84.2 / 88.1	84	88	69.8	9.7	82.1 / 70.3	60.3	71.6
6	6 layers	79.9 / 81	87 / 90.4	87.3	90	76	86.7	85.1 / 76.5	65	82.3
	10 layers	80.7 / 81.6	87.1 / 90.4	87.5	87.5	76.5	87.2	90.2 / 86.3	64.3	83.6
	12 layers	80.4 / 81.2	87.2 / 90.4	88	91.3	76.7	87.4	87.2 / 81.6	65.7	83.4
	14 layers	80.5 / 81.7	87.2 / 90.6	88.1	90.4	78.4	87.8	87.2 / 81.4	68.2	<b>83.8</b>
	18 layers	81.1 / 81.9	87.1 / 90.5	87.7	90.6	79.2	87.3	87 / 82.6	67.2	<b>83.8</b>
7	Tokens Choose	80.2 / 81.2	86.7 / 90.2	87.8	90.1	77.4	87.3	87.6 / 82.4	66.4	83.4
	Experts Choose	80.4 / 81.1	86.8 / 90.2	87.5	90.6	75.9	84.9	88.7 / 83.6	68.6	<b>83.5</b>
8	2-MIXED	80.6 / 81.3	87.1 / 90.5	87.1	90.9	76.7	86.6	88 / 82.4	68.2	<u>83.6</u>
	4-MIXED	80.7 / 80.8	86.7 / 90.2	87.3	90.8	76.8	87.5	88 / 82.4	68.2	<u>83.6</u>
	6-MIXED	80.4 / 81.1	86.8 / 90.2	87.5	90.6	75.9	84.9	88.7 / 83.6	68.6	83.5
	12-MIXED	80 / 80.2	86.7 / 90.1	86.3	90.7	75.5	87.5	87.7 / 82.1	66.8	83.1
	6-BOTTOM	79.9 / 81	86.9 / 90.3	86.9	90.3	76.1	87.1	87.9 / 82.6	66.4	83.2
	6-MIDDLE	80.3 / 80.9	90.6 / 87.2	87.6	90.7	77.6	86.9	89.7 / 85.3	66.4	<b>83.9</b>
	6-MIXED	80.4 / 81.1	86.8 / 90.2	87.5	90.6	75.9	84.9	88.7 / 83.6	68.6	83.5
	6-MIXED*	80.2 / 81.4	87 / 90.4	87.6	90.8	75.5	86.6	88.2 / 82.8	65.0	83.2
6-TOP	80.5 / 81.1	86.5 / 90	87.6	90.5	77.3	85.8	87.7 / 82.8	67.1	83.4	
9	8 experts	80.4 / 81.4	86.2 / 89.8	88	90.9	75.7	86.7	88.3 / 83.1	65.7	83.3
	16 experts	80.4 / 81.1	86.8 / 90.2	87.5	90.6	75.9	84.9	88.7 / 83.6	68.6	<b>83.5</b>
	32 experts	80.4 / 81.4	86.8 / 90.2	87.4	91.1	78.3	86.7	87 / 81.4	65.3	83.3
10	$d_{ff}=1536$	80.6 / 81.3	86.8 / 90.2	87.2	90.6	76.5	85.5	87.7 / 82.4	68.6	<u>83.4</u>
	$d_{ff}=3072$	80.4 / 81.1	86.8 / 90.2	87.5	90.6	75.9	84.9	88.7 / 83.6	68.6	<b>83.5</b>
	$d_{ff}=6144$	80.3 / 81.4	87.1 / 90.4	87.8	90.6	76.4	87.3	87.3 / 80.9	67.1	83.3
	$d_{ff}=12288$	80.7 / 81.9	85.9 / 89.7	87.7	90.9	77.9	87.2	85.6 / 79.7	67.1	83.1



Table 17: GLUE results (*Validation* split) for final comparison of BERT, Sparse Mixer (SM), Fast Sparse Mixer (FSM) and other variants for different batch sizes. See the corresponding table for descriptions of each configuration. For each task, we select the best result across the base learning rates  $\{10^{-5}, 5 \cdot 10^{-5}, 10^{-4}, 5 \cdot 10^{-4}, 10^{-3}\}$ . The highest average score for each model (across the three batch sizes) is highlighted in boldface.

Table	Model	Batch	MNLI	QQP	QNLI	SST-2	CoLA	STS-B	MRPC	RTE	Avg.
13	BERT	16	81.3 / 81.8	86.7 / 90.3	88.9	91.1	77.6	87.3	90.5 / 86.8	69.7	<b>84.7</b>
		32	81.2 / 81.5	86.9 / 90.3	88.6	91.3	77.6	87.4	90.4 / 86.5	70	<b>84.7</b>
		64	81.3 / 81.4	87.4 / 90.7	88.7	90.7	77.9	87.5	89.1 / 84.8	70	84.5
	SM	16	80.8 / 81.4	86.9 / 90.2	89.3	91.5	79.2	87.7	90 / 85.8	69.7	84.8
		32	80.7 / 81.4	86.9 / 90.3	88.7	90.6	79.3	87.7	90.4 / 86	70.4	84.8
		64	80.7 / 81	87.1 / 90.5	89.1	90.9	79	88.1	90.4 / 86.3	72.2	<b>85.0</b>
14	SM $cf=0.5$ (FSM)	16	81.2 / 81.5	90.3 / 86.8	89.0	90.9	78.7	87.5	90.2 / 86.3	69.7	<b>84.7</b>
		32	80.8 / 81.1	90.4 / 86.9	89.0	90.4	78.6	87.9	90.8 / 86.8	68.6	<b>84.7</b>
		64	80.6 / 81.2	90.5 / 87.3	88.5	90.9	78.8	88.7	89.6 / 85	69	84.6
	SM $g=2048$	16	80.8 / 81.7	86.6 / 90.2	88.8	90.8	78.3	88	89.1 / 84.3	70.4	<b>84.5</b>
		32	80.5 / 81.6	86.6 / 90.3	88.5	90.5	77.7	87.9	89.4 / 85	69.3	84.3
		64	81.2 / 81.7	87.1 / 90.4	88.6	90.5	78.2	88.7	88.8 / 84.1	68.6	84.4
	SM $g=1024$	16	80.1 / 80.7	86.8 / 90.2	88.3	91.7	76.4	86.9	88.4 / 83.3	68.6	83.8
		32	80.7 / 81	86.9 / 90.3	88.2	90.6	77.3	87.3	88.7 / 83.6	68.6	83.9
		64	80.3 / 80.9	90.4 / 86.9	88.2	90.5	78.2	87.7	88.5 / 83.6	70.4	<b>84.1</b>
	SM $cf=0.75$ , $g=2048$	16	80.1 / 81.1	86.8 / 90.4	88.4	90.9	76.4	87.7	88.6 / 83.8	67.9	83.8
		32	80.6 / 80.9	87 / 90.4	88.2	90.8	76.6	88.5	88.3 / 83.6	68.6	84.0
		64	80.1 / 81.3	87.3 / 90.6	88.4	91.3	78	88.2	89 / 84.3	69	<b>84.3</b>
15	BERT-12	16	80.7 / 81.2	90.5 / 87	88.2	90.8	78.1	87	88.7 / 83.8	69	<b>84.1</b>
		32	80.9 / 81.3	87.1 / 90.5	88.2	91.2	78.4	87.1	88 / 82.8	65.3	83.7
		64	80.9 / 80.7	86.5 / 90.1	88.5	90.9	79.1	87.2	87.4 / 81.8	65.7	83.5

Table 18: SuperGLUE results (*Validation* split) for final comparison of BERT, Sparse Mixer (SM), Fast Sparse Mixer (FSM) and other variants for different batch sizes. See the corresponding table for descriptions of each configuration. We report macro-F1 scores for CB, micro-F1/exact match scores for MultiRC, F1/exact match scores for ReCoRD, and accuracy scores for all other tasks. For each task, we select the best result across the base learning rates  $\{10^{-5}, 5 \cdot 10^{-5}, 10^{-4}, 5 \cdot 10^{-4}, 10^{-3}\}$ . The highest average score for each model (across the three batch sizes) is highlighted in boldface.

Table	Model	Batch	BoolQ	CB	COPA	MultiRC	ReCoRD	RTE	WiC	Avg.
13	BERT	16	74.6	86.4 / 85.7	58	74.1 / 26.2	68.6 / 52.2	65	65.7	<b>65.7</b>
		32	72.9	85 / 85.7	61	73.7 / 25.6	70.4 / 54.4	58.5	67.9	65.5
		64	71.3	75.2 / 80.4	66	71.7 / 21.3	69 / 52.7	62.5	67.9	63.8
	SM	16	74.4	93.3 / 92.9	62	72.4 / 22.5	65.9 / 49.2	64.6	66.5	<b>66.4</b>
		32	73.4	86.5 / 87.5	62	72.8 / 23.4	66.3 / 49.6	67.9	66	65.5
		64	72.4	89.7 / 89.3	59	72.6 / 23.3	65.7 / 48.9	68.6	61.8	65.1
14	SM $cf=0.5$ (FSM)	16	73.5	85.2 / 85.7	69	71.6 / 21.1	65.6 / 48.8	67.9	67.7	<b>65.6</b>
		32	74.3	82.3 / 85.7	56	71.8 / 21.5	63.8 / 46.9	67.1	62.4	63.2
		64	73.2	87.8 / 87.5	58	70.1 / 19.9	65.3 / 48.5	68.2	62.7	64.1
	SM $g=2048$	16	74.4	85.7 / 86.1	64	70.6 / 20	63.2 / 46.2	66.8	61.4	63.8
		32	74.1	82.8 / 83.9	63	70.7 / 20.9	63.6 / 46.7	66.8	62.2	63.5
		64	74.2	85.2 / 89.3	64	71.1 / 20.8	66.6 / 49.9	69	60.7	<b>65.1</b>
	SM $g=1024$	16	73.9	78.7 / 80.4	63	70 / 18.7	62.8 / 45.8	64.3	63.5	62.1
		32	73.4	86.6 / 85.7	64	70.1 / 18.4	64.5 / 47.6	66.4	61.4	63.8
		64	73.6	86.9 / 85.7	61	69.2 / 19.4	64.8 / 47.9	68.6	63	<b>64.0</b>
	SM $cf=0.75$ , $g=2048$	16	73.1	92 / 89.3	67	69.5 / 19.9	62.4 / 45.4	67.1	66.1	<b>65.2</b>
		32	73	87.7 / 89.3	60	69.6 / 19.9	63.9 / 46.9	66.4	64	64.1
		64	72.4	80.1 / 82.1	62	69 / 18.9	65 / 48.1	67.1	63.3	62.8
15	BERT-12	16	73.9	90.5 / 92.9	61	65.3 / 9.5	48.5 / 32	66.8	59.6	60.0
		32	72.5	92.3 / 92.9	58	69.6 / 15.5	50 / 33.3	65	60.2	<b>60.9</b>
		64	70.1	87.8 / 91.1	66	64.9 / 6.8	45.4 / 29.5	65.7	61	58.8

Table 19: Optimizing fine-tuning learning protocols for MoE models. The default model is repeated in several rows: "0.2 ex dropout", "Default LR" (learning rate), " $cf=1.$ ", and "Fine-tune All". The "Default LR" range is  $\{10^{-5}, 5 \cdot 10^{-4}, 10^{-4}\}$ , while the "Large LR" range is  $\{10^{-4}, 5 \cdot 10^{-4}, 10^{-3}\}$ . For "Fine-tune All", we fine-tune all layers; for "Freeze MoE", we fine-tune all but the MoE layers; and for "Dense MLP", we only fine-tune the dense MLP sublayers. The top average scores are highlighted in boldface.

Configuration	MNLI	QQP	QNLI	SST-2	CoLA	STS-B	MRPC	RTE	Avg.
0.0 ex dropout	80 / 80.8	87 / 90.4	88	89.9	75.7	87.1	86.1 / 79.9	66.1	82.8
0.1 ex dropout	80.2 / 81.3	87.1 / 90.3	87.7	90	75.8	87	86.3 / 80.4	65.7	82.9
0.2 ex dropout	80.7 / 81.3	86.9 / 90.3	87.9	90.6	76.8	86.8	86.1 / 79.7	66.8	<b>83.1</b>
0.3 ex dropout	80.5 / 81.6	87 / 90.3	87.9	90.4	76.2	86.7	86.1 / 80.1	66.1	83.0
0.4 ex dropout	80.6 / 81.5	86.8 / 90.3	88.2	90.5	76	87.5	86.5 / 80.4	65.3	<b>83.1</b>
Default LR	80.7 / 81.3	86.9 / 90.3	87.9	90.6	76.8	86.8	86.1 / 79.7	66.8	83.1
Large LR	80.4 / 81.1	86.8 / 90.2	87.5	90.6	75.9	84.9	88.7 / 83.6	68.6	<b>83.5</b>
$cf=1.$	80.7 / 81.3	86.9 / 90.3	87.9	90.6	76.8	86.8	86.1 / 79.7	66.8	83.1
$cf=2.$	80.1 / 81.1	86.8 / 90.2	88	90.7	77.4	86.9	87 / 82.1	66.4	<b>83.3</b>
Fine-tune All	80.7 / 81.3	86.9 / 90.3	87.9	90.6	76.8	86.8	86.1 / 79.7	66.8	<b>83.1</b>
Freeze MoE	80.4 / 80.9	86.9 / 90.2	88.2	90.9	75.3	86.6	85.9 / 78.9	67.1	82.8
Dense MLP	78.8 / 79	89.9 / 86.4	87.3	90.3	69.2	84.4	73.5 / 83.2	63.2	80.5

Table 20: Model configurations. Following the Base convention for both BERT and Sparse Mixer, we set  $d_{ff} = 4d_h$  and the number of self-attention heads to  $d_h/64$ . Roughly following the Sparse Mixer Base design, we set the number of MoE and attention layers to be roughly 1/3-1/4 of the larger models and no less than 2 for the smaller models. We increase the number of experts for the larger models.

Name	BERT			Sparse Mixer					
	Layers	$d_m$	$d_{ff}$	Layers	$d_m$	$d_{ff}$	Attention	MoE	Experts
Base	2	256	1024	2	256	1024	2	2	16
	4	256	1024	4	256	1024	2	2	16
	4	512	2048	4	512	2048	2	2	16
	8	512	2048	8	512	2048	4	4	16
	12	768	3072	14	512	2048	4	4	16
	18	768	3072	18	768	3072	6	6	32
Large	24	1024	4096	24	1024	4096	6	6	64

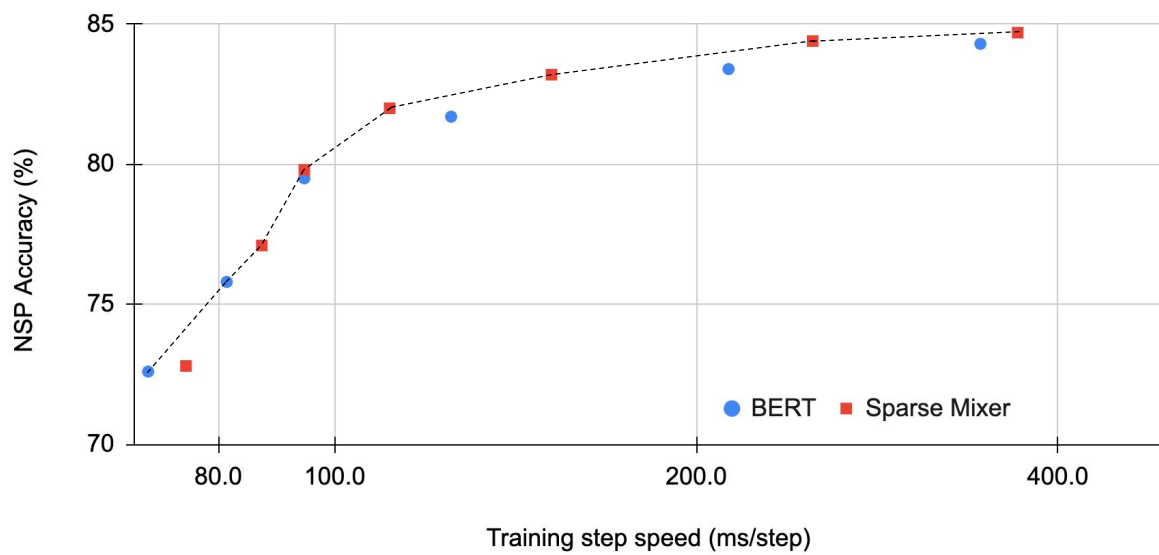


Figure 4: NSP pre-training Speed-accuracy trade-offs for Sparse Mixer and BERT. The dashed line shows the Pareto efficiency frontier, indicating the best trade-offs.